Fundamental understanding of the Di-Air system (an alternative NO_x abatement technology). I: The difference in reductant pre-treatment of ceria

Wang, Yixiao; Makkee, Michiel

DOI
10.1016/j.apcatb.2017.04.054

Publication date
2018

Document Version
Final published version

Published in
Applied Catalysis B: Environmental

Applied Catalysis B: Environmental 223 (2018) 125–133

Contents lists available at ScienceDirect

Applied Catalysis B: Environmental

journal homepage: www.elsevier.com/locate/apcatb

Fundamental understanding of the Di-Air system (an alternative NO_x abatement technology). I: The difference in reductant pre-treatment of ceria

Yixiao Wang, Michiel Makkee*

Catalysis Engineering, Chemical Engineering Department, Delft University of Technology, Julianalaan 136, 2628 BL Delft, The Netherlands

ARTICLE INFO

Article history:
Received 1 October 2016
Received in revised form 6 April 2017
Accepted 20 April 2017
Available online 27 April 2017

Keywords:
Ceria
Hydrocarbon oxidation/cracking
CO oxidation
Di-Air
TAP

ABSTRACT

Toyota's Di-Air DeNO$_x$ system is a promising DeNO$_x$ system to meet NO$_x$ emission requirement during the real driving, yet, a fundamental understanding largely lacks, *e.g.* the benefit of fast frequency fuel injection. Ceria is the main ingredient in Di-Air catalyst composition. Hence, we investigated the reduction of ceria by reductants, *e.g.* CO, H_2, and hydrocarbons (C_3H_6 and C_3H_8), with Temporal Analysis of Product (TAP) technique. The results show that the reduction by CO yielded a faster catalyst reduction rate than that of H_2. However, they reached the same final degree of ceria reduction. Hydrocarbons generated almost three times deeper degree of ceria reduction than that with CO and H_2. In addition, hydrocarbons resulted in carbonaceous deposits on the ceria surface. The total amount of converted NO over the C_3H_6 reduced sample is around ten times more than that of CO. The deeper degree of reduction and the deposition of carbon by hydrocarbon explain why hydrocarbons are the most powerful reductants in Toyota's Di-Air NO$_x$ abatement system.

1. Introduction

In the European Union (EU) the regulated NO$_x$ emissions have decreased over the past two decades. Nevertheless, 9% of EU-28 urban live in areas in which NO$_x$ concentrations still exceed regulated NO$_x$ standards in 2013, according to the Air quality for EU in 2014 (source European Environmental Agency [1]). In the European Union, around 40% of the NO$_x$ emissions are from the traffic sector [2]. Due to the limited effectiveness of currently available NO$_x$ abatement technologies, as of September 2017, 2.1 times the current Euro 6 NO$_x$ emission standard (as measured with the conservative, less demanding ECE & EDCE test cycle) is allowed for in the newly established real driving emission (RDE) test [3]. In the future NO$_x$ emission will become even more stringent, which clearly indicates that currently available technologies: Three-way catalyst (TWC), Urea-SCR (Selective Catalytic Reduction), Lean NO$_x$ Traps (NSR – NO$_x$ Storage & Reduction), still need significant improvements. Therefore, efficient exhaust emissions after-treatment technologies are highly demanded. Recently, Bisaiji et al. (Toyota company) developed the Di-Air system (Diesel DeNO$_x$ System by Adsorbed Intermediate Reductants). Short rich and lean time intervals are created by high frequency directly injecting hydrocarbons (diesel fuel injection) into the exhaust system upstream of a typical NSR catalyst (Pt/Rh/Ba/K/Ce/Al_2O_3) [4,5]. The Di-Air system has shown promise to meet future NO$_x$ emission standards under realistic driving test conditions.

In the Di-Air system, hydrocarbons are the most powerful reductants in the reduction of NO$_x$, as compared to other reductants, *e.g.* CO and H_2 [5]. However, the mechanism is still not clear. Before system optimisation with regard to catalyst formulation and fuel injection strategies, the principle and fundamental understanding of the Di-Air system are a prerequisite.

Ceria is an essential catalyst ingredient in the Di-Air system, as it acts as an oxygen buffer. The ceria lattice oxygen can react with hydrocarbons, CO, and H_2 under rich conditions [6]. In our research, a commercially available model Zr and La-doped ceria is used. The Zr–Ce solid solution, in which zirconium partially replaces cerium, provides a higher (hydro)thermal stability and a larger oxygen storage capacity [7], whereas lanthanum is present to increase the rate of oxygen bulk diffusion [8]. A reduced ceria can selectively convert NO into (di)nitrogen (N_2), even in the presence of an excess of oxygen [9].

In this study, we mainly focus on the investigation of the reduction behavior of the Zr and La-doped ceria catalyst, using H_2, CO, C_3H_6, and C_3H_8 as reductants. Temporal Analysis of Products (TAP) is used to ascertain the reaction between the reductants and the

* Corresponding author.
E-mail address: m.makkee@tudelft.nl (M. Makkee).

http://dx.doi.org/10.1016/j.apcatb.2017.04.054

catalyst. Since high intensity of hydrocarbon reductant injections is applied in the Di-Air system, these pulses will create a locally reduced environment. Therefore, all the experiments in this study are performed in the absence of gas-phase O_2. The performed experiments will provide an illustrative model of the product evolution as a function of the catalyst-reduction degree in an attempt to obtain a fundamental understanding of the Di-Air system. To demonstrate the effect of different reductants on NO reduction, NO reduction is performed over the Zr–La doped ceria by pre-treatment of various reductants. The re-oxidation of the reduced ceria by NO is identical to the reduction of NO into N_2 over reduced ceria.

2. Experimental

The catalyst used is a commercial Zr–La doped ceria (BASF company, denoted as ceria) which serves as a core component in the Di-Air catalyst formulation. The characterisation of this Zr–La doped ceria is described in more detail elsewhere [10].

2.1. Pulses experiment in TAP

The pulse experiments were carried out in an in-house developed TAP (Temporal Analysis of Products) reactor. Small gas pulses, typically in the order of 1×10^{15} molecules, were introduced in a small volume (1 mL) upstream of the catalyst packed bed reactor. The produced pressure gradient over the catalyst packed bed thereby caused the molecules to be transported through the packed bed to the ultra-low vacuum at the opposite side of the reactor bed. Depending on the actual amount of molecules pulsed, the transport can be purely Knudsen diffusion. In other words, the molecules will only interact with the 'walls' (catalyst surface and reactor walls) of the system and not with each other. Upon interaction with the catalyst, the molecules can be converted into different products. The evolution of the reactant and product molecules are tracked (one mass at a time) in time with a high resolution of 10 kHz by means of a mass spectrometer. More details about TAP can be found in elsewhere [9,11].

21.2 mg ceria (100–250 μm, BET surface area 65 m^2/g) was used in the TAP reactor. In all experiments a starting pulse size of approximately 1.6×10^{15} molecules (excluding internal standard gas) was used, the pulse size gradually decreased during an experiment as the reactant was pulsed from the closed and calibrated volume of the pulse-valve line. Prior to the reduction, the ceria was firstly re-oxidised at the same temperature at which the reduction was performed, using pulses of 80 vol.% O_2 in Ar until a stable O_2/Ar signal ratio was obtained. The reduction was carried out by pulsing reductant of either 80 vol.% C_3H_6 in Ne or 80 vol.% C_3H_8 in Ne or 80 vol.% CO in Ar or 67 vol.% H_2 in Ar until a stable reactant and product to the internal standard signal ratio was achieved, indicating that the ceria was equilibrated. NO pulse experiments were performed using 80 vol.% NO in Ar.

The consumption of the oxygen species from the ceria during H_2, CO, C_3H_8, and C_3H_6 pulses experiments was calculated using the following mass balance:

$$n_{O,consumed} = n_{H_2O,obs} + n_{CO,obs} + 2n_{CO_2,obs} \quad (1)$$

where n is the number of molecules or atoms of the specified species observed (obs), consumed, or introduced (in).

The number of carbon species deposited on the doped ceria surface in the C_3H_6 pulse experiments was calculated using the following mass balance:

$$n_{C,deposited} = 3n_{C_3H_6,in} - 3n_{C_3H_6,obs} - n_{CO,obs} - n_{CO_2,obs} \quad (2)$$

Similarly, the number of carbon species deposited on the ceria surface in the C_3H_8 pulse experiments was calculated using the following mass balance:

$$n_{C,deposited} = 3n_{C_3H_8,in} - 3n_{C_3H_8,obs} - 3n_{C_3H_6,obs} - n_{CO,obs} - n_{CO_2,obs} \quad (3)$$

The number of carbon species during CO pulse experiments on the ceria surface was calculated using the following material balance:

$$n_{C,deposited} = n_{CO,in} - n_{CO,obs} - n_{CO_2,obs} \quad (4)$$

The average particles size of ceria was around 5 nm, based on XRD and TEM analyses [10]. The hypothetical ceria layers concept was used in order to obtain insight in the reductant reactivity as a function of the degree of ceria reduction (surface oxidation state).

As the ceria (111) crystal plane is a stoichiometric O–Ce–O tri-layer stacked along the [111] direction, we regarded each O–Ce–O tri-layer as one hypothetical ceria layer (0.316 nm). Assuming a perfect cubic crystal structure of ceria (size 5.0 nm), the total number of hypothetical ceria layers were determined to be 16 (111) layers. Assuming that Zr is identical to Ce, a maximum of 25% of the number of O ions in each crystal layer can be reduced, the number of reducible oxygens in one hypothetical ceria layer with BET surface area of 65 m^2/g is calculated to be $5.4 \times 10^{18}/21.2\ m_{Cat}$. Details can be found in [9,10].

2.2. In situ *Raman*

In situ Raman spectra (Renishaw, 2000) were recorded using a temperature controlled *in situ* Raman cell (Linkam, THMS 600). Ten scans were collected for each spectrum in the 100–4000 cm^{-1} range using continuous grating mode with a resolution of 4 cm^{-1} and scan time of 10 s. The spectrometer was calibrated daily using a silicon standard with a strong absorption band at 520 cm^{-1}. The spectra were recorded during the flow of C_3H_6 (1000 ppm in N_2, flow rate 200 mL/min).

3. Results

3.1. Reduction of ceria by CO

Fig. 1 showed the result of CO pulses experiment at 580 °C. During the initial period (pulse number 0–2000, Fig. 1A), the CO was completely converted into CO_2. Pulse number 2000 corresponded to 0.4 hypothetical reduced ceria layers (Fig. 1B). After this initial period, the CO conversion and CO_2 production progressively decreased, but never reached a zero conversion level during the duration of the experiment. In the CO oxidation process, only oxygen from the catalyst can be consumed, as can be seen from the oxygen balance (Table 2). No carbon deposits were observed on the catalyst within experimental error.

Similar results were obtained at 400–500 °C (not shown), but CO conversion did never reach full conversion in this temperature window. At 200 °C and lower, no significant CO oxidation activity was observed (not shown). The number of hypothetical reduced ceria layers (1.2–1.0) were relatively constant in the 400–580 °C temperature window (Table 2).

3.2. Reduction by H_2

Fig. 2 shows the result of H_2 pulses experiment at 560 °C For a very short period (pulse number 0–210, Fig. 2A), hydrogen conversion was relatively high without a clear desorption of water. In contrast to the CO experiment, the H_2 conversion did not accomplish full conversion. The H_2 conversion and H_2O production decreased progressively during the remainder of the experiment

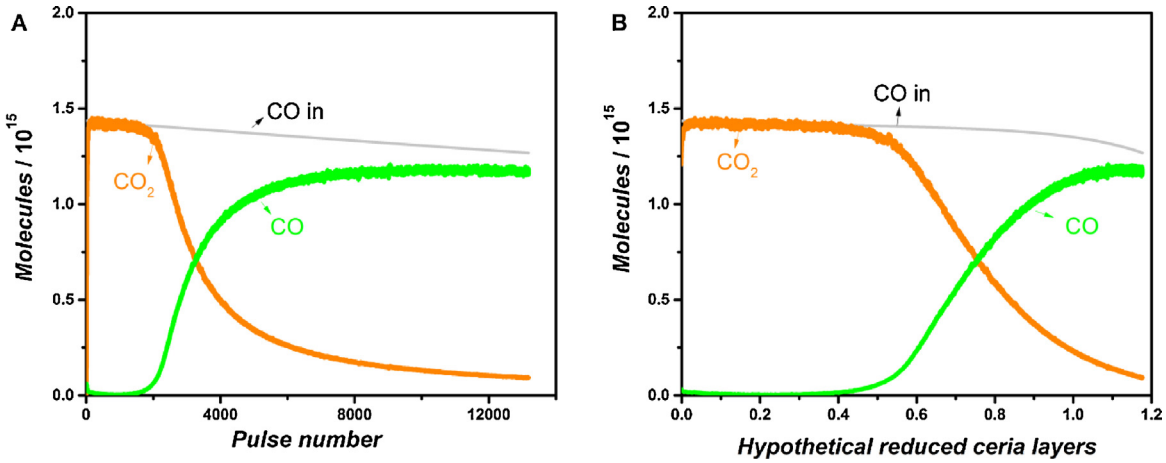

Fig. 1. CO pulse experiment over a pre-oxidised ceria at 580 °C, (A) with pulse number and (B) with hypothetical reduced layers.

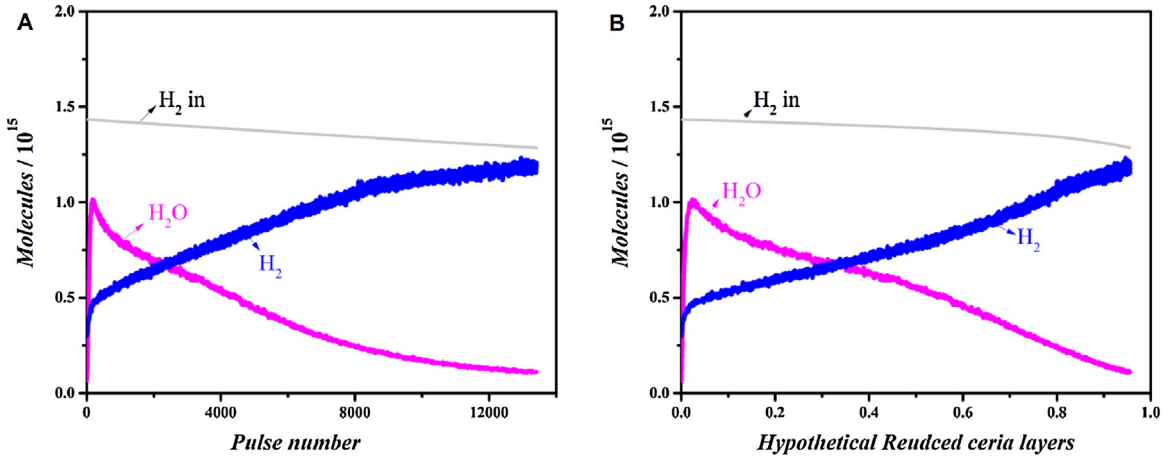

Fig. 2. H_2 pulse experiment over pre-oxidised ceria at 560 °C, (A) with pulse number (B) with hypothetical reduced layers.

Table 1
Definition of different phases during the C_3H_6 and C_3H_8 pulses in TAP.

Phases	Hydrocarbon reactivity
I	Initial full conversion of hydrocarbon
II	Hydrocarbon conversion drop
III	Hydrocarbon conversion increase
IV	Period of constant hydrocarbon conversion
V	Hydrocarbon conversion decrease

(pulse number 210–end, Fig. 2B). The number of extracted oxygen atoms, characterised as the number of hypothetical reduced ceria layers, was at the end of the experiment around 1 reduced layer (Table 2).

3.3. Reduction by C_3H_6

Fig. 3 showed the result of C_3H_6 pulses experiment at 580 °C. Different phases were applied to define C_3H_6 reactivity profiles with pulse number, as shown in Table 1. The definition of different phases was also applied to C_3H_8 reactivity in Fig. 5.

Fig. 3A showed the product and reactants evolution *versus* pulse number during C_3H_6 pulses. In phase I (pulse number 0–80), a high activity was observed, where predominantly total oxidation products, *i.e.*, CO_2 and H_2O were formed. The H_2 formation was observed from the start of the experiment, while CO production was initially zero. Both H_2 and CO production increased during this phase I. After this short highly active phase I, C_3H_6 conversion rapidly declined in phase II (pulse number 80–500). In phase III and IV (pulse number 400–8000) predominantly partial oxidation took place and mainly CO and H_2 were observed. From pulse number 2800–8000 (phase III), C_3H_6 conversion increased to full conversion. H_2 was the major product and the formation of CO declined with time in this phase III. In phase V (pulse number 8000–end), both C_3H_6 conversion and H_2 production declined. The H_2 production and C_3H_6 conversion remained persistent although at a low level no CO was observed.

Some carbon (Fig. 3C) started to deposit on the surface from phase II (determined from the carbon mass balance). Siginicant

Table 2
Summary of the number of deposited carbon and extracted oxygen atoms in the ceria reduction experiments.

	Deposited carbon		Extracted oxygen	
	Atoms	wt.%/g_{Cat}	Atoms	HRCL[a]
580 °C C_3H_6	3.1×10^{19}	2.9	1.5×10^{19}	2.6
560 °C C_3H_6	3.4×10^{19}	3.2	1.1×10^{19}	1.8
540 °C C_3H_6	3.3×10^{19}	3.1	1.1×10^{19}	1.8
500 °C C_3H_6	1.9×10^{19}	1.8	9.2×10^{18}	1.7
580 °C C_3H_8	1.5×10^{19}	1.4	1.5×10^{19}	2.6
540 °C C_3H_8	1.1×10^{19}	1	0.9×10^{19}	1.7
580 °C CO	–	–	6.3×10^{18}	1.2
500 °C CO	–	–	6.0×10^{18}	1.1
400 °C CO	–	–	5.4×10^{18}	1.0
560 °C H_2	–	–	5.2×10^{18}	1.0

[a] Hypothetical reduced ceria layers.

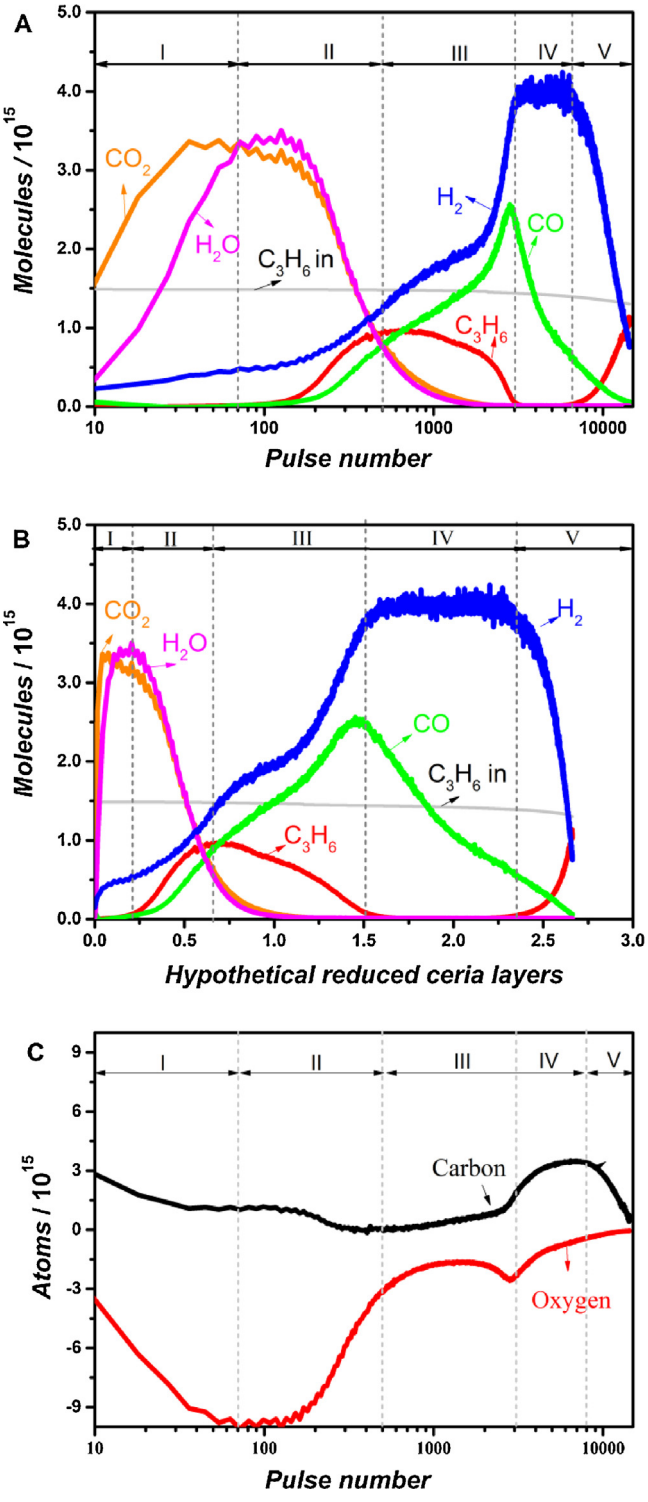

Fig. 3. C_3H_6 pulse experiment over a pre-oxidised ceria at 580 °C, (A) product and reactants evolution *versus* pulse number, (B) product and reactants evolution *versus* hypothetical reduced ceria layers, and (C) carbon and oxygen balance *versus* pulse number.

amounts of carbon depositions were observed when the CO formation started to decline, while H_2 formation persisted (phase IV). C_3H_6 showed full conversion during phase I and IV, corresponding to 0–0.25 and 1.5–2.7 hypothetical reduced ceria layers, respectively, as shown in Fig. 3B.

The estimated oxygen atom consumption and carbon atom deposition during the C_3H_6 pulse experiment at 580 °C were calculated to be 1.5×10^{19} and 3.1×10^{19} carbon atoms (2.9 wt.%), respectively, shown in Table 2. Fig. 4 showed the C_3H_6 conversion *versus* pulse number in a temperature window between 500 and 580 °C. Similar C_3H_6 reactivity profiles were observed, although the overall reactivity of C_3H_6 decreased, when reaction temperature declined. No significant C_3H_6 activity and reduction of ceria were observed below 500 °C. Table 2 summarised the oxygen consumption (hypothetical reduced ceria layers) and carbon deposits for the 500–580 °C temperature window.

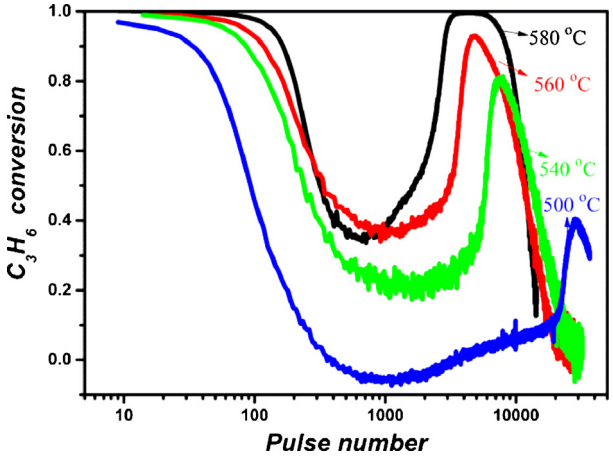

Fig. 4. C_3H_6 conversion *versus* pulse number during C_3H_6 pulse experiments over a pre-oxidised ceria at the indicated temperatures.

3.4. Reduction by C_3H_8

Fig. 5 showed the result of C_3H_8 pulses experiment at 580 °C. As compared to C_3H_6, C_3H_8 in phase I did not have a full conversion time interval). Fig. 5A shows the product and reactant evolution *versus* pulse number during C_3H_6 pulses. In phase II (pulse number 80–1000), a short period of a higher activity (up to 40% conversion) was observed, where predominantly total oxidation products, *i.e.*, CO_2 and H_2O, were formed. The H_2 formation was observed from the start of the experiment, while CO production was initially zero, both H_2 and CO production increased during this phase II. The C_3H_8 conversion declined during phase II and increased during phase III (up to 60% conversion). In phase III and IV, partial oxidation took place and CO and H_2 were observed, while C_3H_6 was only observed during phase III. The level of C_3H_8 conversion was substantially lower as compared to that of C_3H_6.

During the partial oxidation time interval (phase III, IV, and V), CO and H_2 were observed as the main products. The reaction rate increased with pulse number during phase III and IV. During phase III the C_3H_6 production, resulting from the dehydrogenation of C_3H_8, increased progressively but vanished towards the end of phase III. A maximum in CO production was observed when the activity for the dehydrogenation reaction vanished. In this the partial oxidation period, in contrast to the C_3H_6 pulse experiment, the C_3H_8 conversion was never complete. Initially, the C_3H_8 conversion was around 10% and reached a maximum conversion of 60% at the point of maximum CO production (Fig. 6). Following the maximum in the CO production, the C_3H_8 conversion and H_2 production also reached their maximum level (phase IV, Fig. 5). In phase V, the C_3H_8 conversion and CO and H_2 production declined. CO evolution stopped after pulse number 22,000, while C_3H_8 conversion and H_2 production remained persistent at a low level. At a temperature of 500 °C and lower, the reactivity of C_3H_8 was negligible or none (not shown).

As shown in Table 2, the amounts of deposited carbon ranged from 1.4 to 0.9 wt.% for temperatures from 580 °C to 540 °C, which

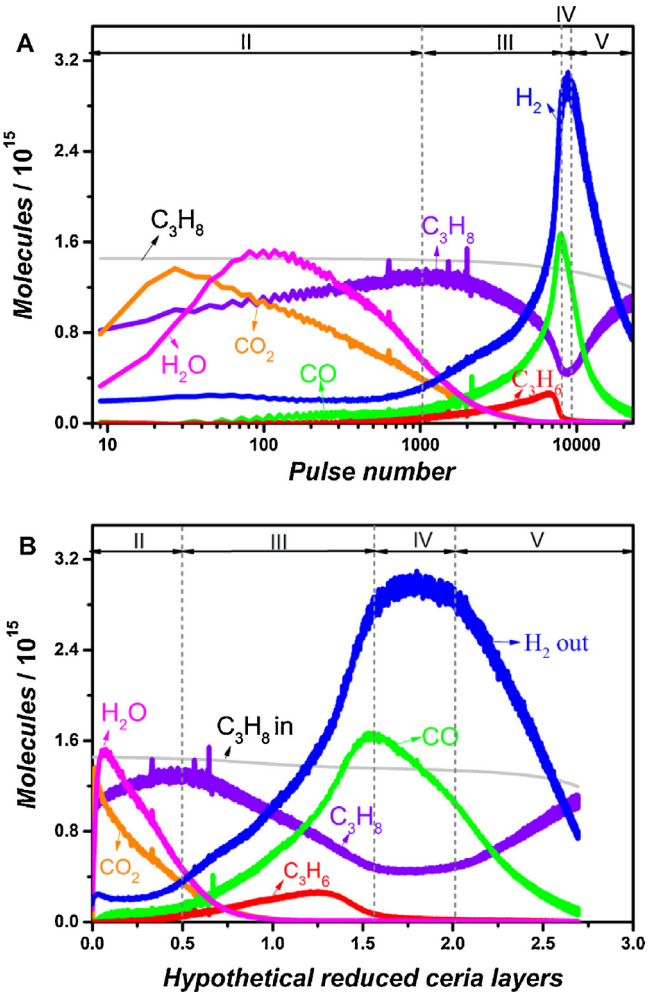

Fig. 5. C_3H_8 pulse experiment over a pre-oxidised ceria at 580 °C: (A) product and reactants evolution with pulse number and (B) product and reactants evolution *versus* hypothetical reduced layers.

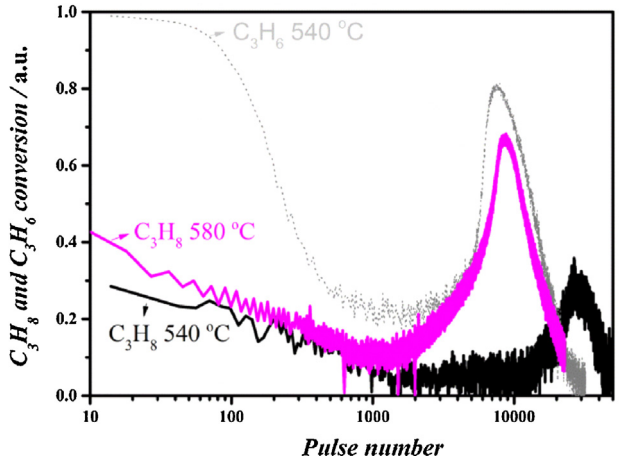

Fig. 6. C_3H_8 conversion *versus* pulse number during C_3H_8 pulse experiments over a pre-oxidised ceria at the indicated temperatures.

were less than that of propene. C_3H_8 was able to reduce the catalyst as far as 2.7 hypothetical reduced ceria layers, which was the same as that for C_3H_6 at 580 °C, but the required number of pulses, however, was around double than that of C_3H_6.

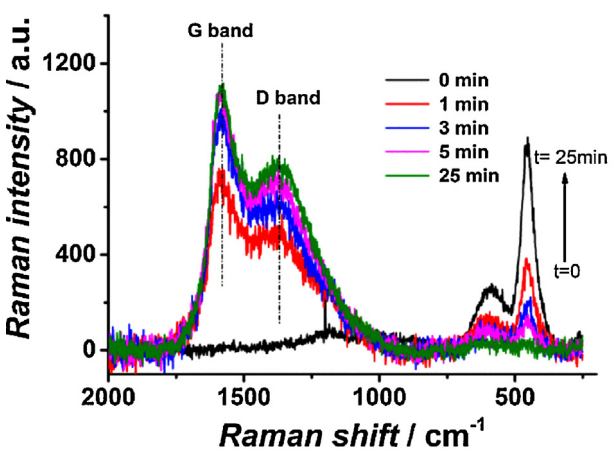

Fig. 7. Raman spectra during C_3H_6 flow over ceria catalyst at 580 °C.

In Fig. 6, the C_3H_8 conversion was plotted *versus* pulse number at 580 and 540 °C, respectively. In the initial total oxidation period, approximately 40% and 30% C_3H_8 conversion were achieved at 580 and 540 °C, respectively. The incremental C_3H_8 conversion in phase II and III was sensitive to the temperature, which shifted to higher pulse numbers with decreasing temperature and its maximum C_3H_8 conversion decreased from 65 to 30%, when the temperature decreased from 580 to 540 °C. Compared to C_3H_6 conversion at 540 °C, as indicated dotted gray line in Fig. 6, C_3H_8 was less active and took around two times more pulses than that of C_3H_6 to reach the final state. As shown in Table 2, the amount of deposited carbon during C_3H_8 at 540 °C was around three times less than that for C_3H_6 at the same temperature.

3.5. In situ *Raman experiment of C_3H_6 flow over ceria*

In situ Raman was used to analyse the deposited carbon formed over ceria during C_3H_6 flow at 580 °C. D band and G bands of carbon were observed during the C_3H_6 flow as shown in Fig. 7. The G band corresponded to graphitic in-plane vibrations with E_{2g} symmetry. D band generally was assigned to the presence of defects in and disorder of carbon.

3.6. *Re-oxidation of reduced ceria by NO*

In order to investigate the effect of the reduction degree as well as the amount of deposited carbon on the NO reduction into (di)nitrogen (N_2) over (pre-reduced) La–Zr doped ceria, NO was used in the re-oxidation of CO, H_2 (not shown), C_3H_8, and C_3H_6 pre-reduced La–Zr doped ceria, as illustrated in Fig. 8 at 540 °C.

For the CO (and H_2) pre-treated samples, a full NO conversion was obtained till pulse number 2340. The total amount of NO converted was around 6.8×10^{18} molecules. For the propane pre-treated ceria, complete NO conversion maintained approximately till pulse number 1200. The total amount of NO converted was around 2.9×10^{19} molecules. For the C_3H_6 pre-treated ceria sample, however, NO showed full conversion up to pulse number 5600, followed by a conversion decline to 76% at pulse number 9000. Subsequently, the NO conversion for the C_3H_6 increased to full conversion till pulse number 40,000. NO lost its activity after pulse number 97,300. The total amount of NO being converted was around 7.6×10^{19} molecules.

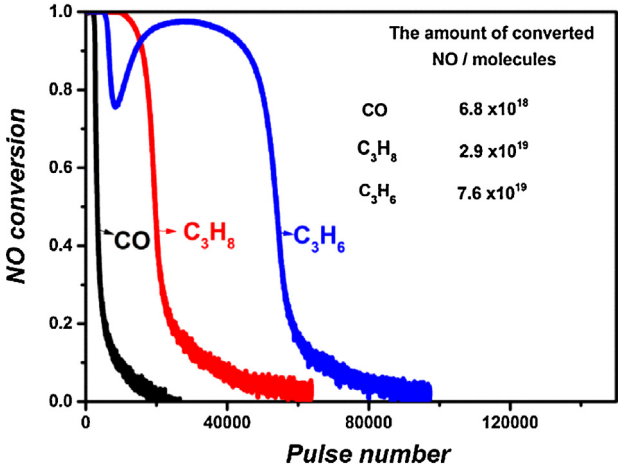

Fig. 8. NO reduction over CO and hydrocarbons pre-reduced ceria at 540 °C.

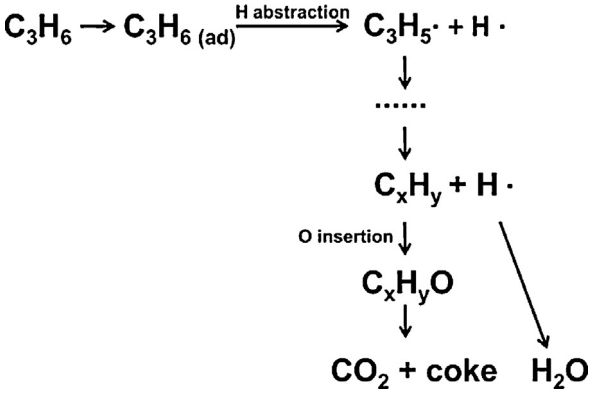

Scheme 1. C_3H_6 activation steps for the formation of CO_2 and H_2O.

4. Discussion

4.1. Reduction of ceria by CO and H_2

The CO pulse experiments over Zr–La doped ceria resulted in an overall catalyst reduction of around on average one hypothetical reduced ceria layer in the 400–580 °C temperature window (Table 2), indicating that a complete surface layer of Zr–La doped ceria can be reduced by CO. The extraction of one oxygen resulted in the reduction of two Ce^{4+} ions into two Ce^{3+} ions. The oxidation of CO to CO_2 can be described as:

$$CO + 2Ce^{4+} + O^{2-} \rightarrow CO_2 + 2Ce^{3+} + \blacksquare \quad (\blacksquare \text{oxygenvacancy}) \qquad (5)$$

The CO_2 production was due to the oxidation of CO by oxygen species (originating) from the ceria lattice since there was no gas-phase O_2 present during the CO pulse experiment. The full CO_2 conversion dropped at the point corresponding to 0.5 hypothetical reduced ceria layers (Fig. 1B), which indicated that the oxygen species generated from surface lattice oxygen had a high activity for the CO oxidation into CO_2. The observed decline in CO activity between 0.5 and 1 hypothetical reduced ceria layers (Fig. 1B) implied that only surface oxygen participated in the CO oxidation.

Significant participation of the disproportionation of CO into carbon and CO_2 ($2CO \rightarrow C + CO_2$) can be excluded, because hardly any deposited carbon was observed and could be quantified for the calculated carbon mass balance (Fig. 1A). The total reduction degree of ceria by CO was not significantly affected by temperatures in the range of 400–580 °C. The reactivity of CO, however, declined as the temperate decreased, since more CO pulses were needed in order to obtain the same reduction degree at low temperatures, *i.e.* 400 °C (*i.e.* 580 °C) (not shown).

The limitation for the reduction of only one hypothetical reduced ceria layer by CO cannot be attributed to the oxygen diffusion since the reduction degree of ceria was not significantly influenced by a temperature between 400 and 580 °C. The role of ceria in the reduction of CO_2 to CO had been widely studied in the field of solar cells [12–14]. CO_2 can also re-oxidise reduced ceria, thereby forming CO. The coexistence of CO and CO_2 in the 0.5–1 hypothetical reduced ceria layer range suggested the presence of an equilibrium between CO, CO_2, Ce^{3+}, and Ce^{4+}, which may limit the obtainable degree of reduction for ceria during CO pulse experiments (Fig. 1B).

For the H_2 pulse experiments, a high H_2 activity was observed from the start of the experiment (Fig. 2) in the absence of any water desorption. This indicated that water or its precursor species were initially stored on the catalyst's surface. H_2 activity dropped immediately after the initial pulses until hardly any conversion was observed when one hypothetical reduced ceria layer was reached. Similar to the CO pulse experiments, when the ceria surface became reduced, the reduced ceria tended to use water or an intermediate to re-oxidise itself [15]. The coexistence of H_2 and H_2O during a whole H_2 pulse experiment suggested the presence of an equilibrium between H_2, H_2O, Ce^{3+}, and Ce^{4+}, which may limit a deeper reduction of ceria by H_2.

4.2. Reduction by hydrocarbons

4.2.1. Reduction by C_3H_6

The reduction of Zr–La doped ceria by C_3H_6 led to an overall 2.7 hypothetical reduced ceria layers at 580 °C (Table 2). Unlike CO and H_2 pre-treatment, the C_3H_6 interaction with the catalyst can be characterised by two types of reactions: complete C_3H_6 oxidation and subsequently C_3H_6 cracking/partial oxidation (Fig. 3).

The initial high conversion to total oxidation products (phase I): CO_2 and H_2O, was most probably due to the high concentration of active surface oxygen species, which were formed through an oxygen activation chain as given in Eq. (6) [16–18]:

$$O_{2(ad)} \overset{+e^-}{\leftarrow} O_2^- \overset{+e^-}{\leftarrow} O_2^{2-} \leftrightarrow 2O^- \overset{+2e^-}{\leftarrow} 2O_{lattice}^{2-} \qquad (6)$$

These active surface oxygen species reacted with C_3H_6 resulting mainly in the formation of H_2O and CO_2 as described in Scheme 1. The adsorbed C_3H_6 was activated by the active oxygen species from oxygen activation chain (Eq. (6)), forming the $C_3H_5^{\bullet}$ and $H^{\bullet}$. Then $H^{\bullet}$ will react with active oxygen species, forming $^{\bullet}OH$. Another $H^{\bullet}$ will be further abstracted from $C_3H_5^{\bullet}$ and to form H_2O from $^{\bullet}OH$. The remained hydrocarbon fragment (C_xH_y) will react with active oxygen species, forming oxygen-containing hydrocarbon intermediate (C_xH_yO), and finally oxidation of some part of C_xH_yO to CO_2, the remained C_xH_yO will be deposited as "coke" as illustrated in Scheme 1.

C_3H_6 conversion dropped (phase II), accompanied by a decline in total oxidation products and the start of C_3H_6 cracking/partial oxidation reaction. The fall of C_3H_6 conversion during phase II was likely caused by less availability of the active surface oxygen species which were largely consumed during phase I. As described in Scheme 2, the adsorbed C_3H_6 will be activated by the active oxygen species, forming the $C_3H_5^{\bullet}$ and $H^{\bullet}$. This $H^{\bullet}$ will react with active oxygen species, forming $^{\bullet}OH$. Another H will be further abstracted from $C_3H_5^{\bullet}$. However, on the reduced catalyst surface (less active surface oxygen), H surface species preferred to recombine with each other to form H_2. The remained hydrocarbon fragment (C_xH_y) will react with active oxygen species, forming oxygen-containing hydrocarbon intermediate (C_xH_yO), and some part of C_xH_yO will be converted to CO, the remained C_xH_yO will be deposited as coke. The

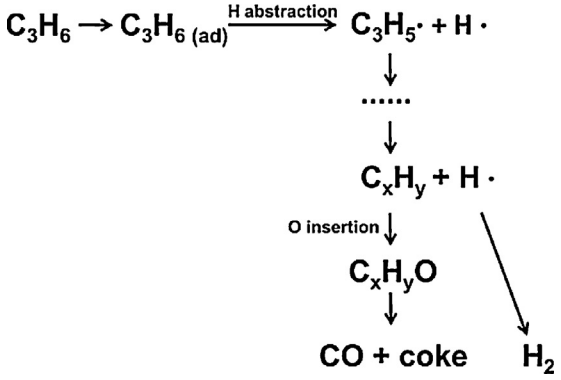

Scheme 2. C_3H_6 activation steps for the formation of CO and H_2.

Scheme 2 was also applied to the C_3H_6 cracking reaction during the phase III. C_3H_6 conversion increased during phase III accompanied by an increased H_2 and CO formation, indicating the main cracking/partial oxidation/dehydrogenation were taking place.

The CO formation arrived at a maximum formation rate at 1.5 hypothetical reduced ceria layers, while CO_2 and H_2O were not observed around 1 hypothetical reduced ceria layer. This observation indicated that the formation of CO consumed oxygen from the bulk of ceria, resulting in a deeper degree of catalyst reduction by C_3H_6, as compared to CO and H_2 treatment. The CO formation declined at the point of 1.5 hypothetical reduced ceria layers and ceased at 2.7 hypothetical reduced ceria layers. This will indicate that the deposited carbon oxidation to CO started to be limited when the catalyst reduced to 1.5 hypothetical reduced ceria layers. This can be explained by the scarceness of surface active oxygen species either due to slow bulk oxygen diffusion or the activation of bulk oxygen to active oxygen species. The formation of CO caused the additional extraction of oxygen from ceria bulk, *i.e.* degree of reduction of the bulk ceria up to 2.7 hypothetical reduced ceria layers (phase V).

The increase of C_3H_6 conversion during phase III was also likely due to the regeneration of active oxygen species from activation oxygen from bulk diffusion to surface, which led to CO formation increasing and less carbon deposition as compared to phase II, based on the carbon mass balance calculations. The CO formation, however, declined from 1.5 hypothetical reduced ceria layers, where still a full C_3H_6 conversion and persistent H_2 formation were observed (phase IV). The full C_3H_6 conversion (C_3H_6 cracking) during phase IV cannot be ascribed to the increased active oxygen species availability. Otherwise, the CO formation rate would increase as well. Another type of species started to play a role in C_3H_6 cracking/partial oxidation (deeper dehydrogenation).

The total amount of carbon deposition till the point of 1.5 hypothetical reduced ceria layers was around 2×10^{18} carbon atoms. Assuming that the carbon structure will be graphene-like structure, the coverage of Zr–La doped ceria by carbon corresponded to roughly 4% of the available surface area. Carbonaceous deposited (coke) that formed on the metal oxides can be regarded as the real catalyst site for (oxidative) dehydrogenation. The formation of deposited carbon was observed from the *in situ* Raman (Fig. 7). The catalytic site on the coke will be the quinone/hydroquinone group on the surface of the coke [19–22], as evidence the formation of D band and G band in Fig. 7. The full C_3H_6 conversion with persistent H_2 formation will be attributed to the deposited carbon and will play a role in the deeper C_3H_6 dehydrogenation. The oxygen transport from ceria bulk will become the catalytically active site on the coke (C_xH_yO), and CO was formed by the oxidation of coke (C_xH_yO). When the number of available lattice oxygen declined, the CO formation declined as well. The deeper dehydrogenation of C_3H_6 will lead to more and more deposited carbon.

Till phase V, C_3H_6 lost its reactivity completely, whereas H_2 formation declined as well from 2.2 hypothetical reduced ceria layers, indicating the deeper dehydrogenation reaction largely slowed down. CO was hardly observed the end, while C_3H_6 conversion and H_2 formation were persistent although at a lower level.

Since the coke with quinone group could be regarded as the catalytic site for the C_3H_6 dehydrogenation, the disappearance of this group might explain the final C_3H_6 deactivation. The oxygen transport from ceria bulk and spillover the deposited carbon will be terminated. The formation of C_xH_yO was largely limited when the catalyst was reduced to around 2.2 hypothetical reduced layers. The oxidation of C_xH_yO to CO was persistent although at a low level.

Carbon deposited will often be regarded as one of the leading causes for the deactivation in hydrocarbon reactions [23]. The amount of deposited carbon on the catalyst surface during the C_3H_6 pulses was around 3.1×10^{19} carbon atoms, which accounted for about 2.9 wt%/g_{Cat}. Assuming that the carbon structure will be graphene-like structure and ceria surface will be flat, the coverage of Zr–La doped ceria by carbon will correspond to roughly 60% of the available surface area. There would be still about 40% of the surface area available. The surface of the ceria with or without carbon deposits will be a network of pores. The blocking of the pores in combination with a slow-down of the oxygen spillover mechanism from the bulk to the surface and over the deposited carbon will be the main reasons for the final lost in the C_3H_6 conversion activities.

Similar C_3H_6 reactivity profiles were also observed at 500–580 °C temperature window. The maximum observed C_3H_6 conversion during the cracking reaction period (phase III) shifted to higher pulse numbers in the 580–500 °C temperature range, as shown in Fig. 4. This observation indicated that more time was needed for the enhanced C_3H_6 reactivity in phase III when the temperature decreased. Such phenomenon also pointed out that the reactivity of C_3H_6 during phase III was likely controlled by the availability of active oxygen species on the surface regenerated by bulk oxygen diffusion, which was affected by temperature. At 400 °C, only complete oxidation to CO_2 and H_2O was observed (no carbon deposition) and could be calculated from the carbon mass balance.

The total amount of reducible oxygen during C_3H_6 oxidation was significantly influenced by the temperature, as shown in Table 2. The number of oxygen atoms extracted in the C_3H_6 pulse experiments declined from 1.5×10^{19} to 0.9×10^{19}, *i.e.* from 2.7 to 1.7 hypothetical reduced ceria layers when the temperature decreased from 580 to 500 °C. The total amount of deposited carbon during the C_3H_6 pulse experiment at 580 °C is twice that of the pulse experiment at 500 °C. At 400 °C, carbon was hardly deposited, and no cracking/partial oxidation/dehydrogenation activities were observed.

4.2.2. Reduction of ceria by C_3H_8

C_3H_8 (Fig. 5), showed the same trend as C_3H_6, although C_3H_8 conversion was lower than that of C_3H_6 during phase I and IV. This indicated that the reaction mechanisms were similar for both saturate and unsaturated hydrocarbons. C—H bond cleavage was easier for the unsaturated C_3H_6 as compared to the saturated C_3H_8 due to either the interaction with the surface through hydrogen bonding or Van der Waals forces for C_3H_8 and more strong electron-rich π orbital interactions on Lewis acid sites for C_3H_6 [24]. The lower reactivity, that C_3H_8 displayed toward oxygen species, did not affect the total amount of oxygen extracted during the whole C_3H_8 pulse experiment. It, however, affected strongly on the amount of carbon deposited on the surface and the time frame to achieve the same degree of ceria reduction. Since the carbon deposition took predominantly place during phase IV, the lower C_3H_8 reactivity led to less carbon deposition. Comparing C_3H_6 and C_3H_8

pre-treatment at 580 °C, the amount of carbon deposited for the C_3H_6 pre-treatment was twice of that for C_3H_8, as shown in Table 2.

The C—H bond cleavage was regarded as the first step in the activation of saturated hydrocarbons (C_3H_8). Due to the initial high concentration of surface active oxygen species in phase II, complete oxidation was observed with the formation of both H_2O and CO_2, similar as illustrated in Scheme 1. The conversion of C_3H_8 decreased during phase II was due to the depletion of active oxygen species on the surface. A gradual increase in the amount of the C_3H_6 dehydrogenation product (Fig. 5) was observed from phase III, where the C_3H_8 conversion was enhanced. Similarly to C_3H_6 pulse experiments (Fig. 3), the C_3H_8 reactivity (Fig. 5) increased during phase III was due to the reformation of surface active oxygen species by the diffusion of oxygen from the bulk of the ceria. Dehydrogenation of C_3H_8 to C_3H_6 was observed from initial of phase III and declined from the end of phase III. C_3H_6 evolution completely vanished from phase IV. The dehydrogenation selectivity of C_3H_8 to C_3H_6 in phase III can be explained by a particular type of reformed active oxygen species, *e.g.* O^-. C_3H_6 formation declined around 1.3 hypothetical reduced layers, indicating that these oxygen species, *e.g.* O^- [25], was less present from 1.3 hypothetical reduced layers.

Identically to the C_3H_6 pulse experiment, the formation of CO during C_3H_8 pulse experiment consumed oxygen from catalyst bulk, *i.e.* deeper reduction of bulk. Deposited carbon started to play a role in C_3H_8 dehydrogenation during phase IV, where C_3H_8 conversion was around 60%.

The maximum C_3H_8 conversion during C_3H_8 the cracking//partial oxidation/dehydrogenation reactions (phase III) shifted to a higher pulse number when the temperature was changed from 580 to 540 °C, as shown in Fig. 6. Similarly to the observation in the C_3H_6 pulse experiments, the reactivity of C_3H_6 during phase III was controlled by the availability of active oxygen species on the surface regenerated by bulk oxygen diffusion, which was temperature dependent. The observed C_3H_8 lost in activity can be explained with the same reasoning as discussed above for C_3H_6.

The total amount of reducible oxygen during C_3H_8 oxidation was significantly influenced by the temperature, as shown in Table 2. The number of oxygen atoms extracted in the C_3H_8 pulse experiments declined from 1.5×10^{19} to 0.9×10^{19}, *i.e.* from 2.7 to 1.7 hypothetical reduced ceria layers as the temperature was lowered from 580 to 540 °C.

4.3. Re-oxidation of reduced ceria with NO

The pre-treatment of ceria by CO, H_2, C_3H_8, and C_3H_6 at 540 °C led to a degree of catalyst reduction corresponding to 1, 1, 1.7, and 1.8 hypothetical reduced ceria layers, respectively. The pre-treatment with C_3H_6 and C_3H_8 additionally resulted in the deposition of 3.3×10^{19} and 1.1×10^{19} carbon atoms, respectively.

The differences observed in the reduction of NO into N_2 over ceria by using either CO, C_3H_8 or C_3H_6 pulses at 540 °C was shown in Fig. 8. CO and H_2 pre-treatments showed only a short time interval, where NO was reduced into N_2. The reduction of NO to N_2 started with oxygen from NO filling an oxygen defect site, followed by N—O bond scission and the recombination, after surface diffusion and migration of N species into dinitrogen (N_2) [9,10]. When all the oxygen defects were refilled, the NO reduction was ended. Both C_3H_6 and C_3H_8 pre-treated reduced ceria were able to convert considerable more NO into N_2 (much longer time interval) as compared to CO and H_2 pre-reductions. The pre-treatment of C_3H_6 and C_3H_8 resulted in a deeper catalyst reduction and more deposited carbon. These carbon deposits acted as buffered reductant: the oxidation of deposited carbon by active oxygen species from ceria lattice recreated the oxygen defect sites that can be again used for additional NO conversion. C_3H_6 pre-treatment exhibited a longer period of NO reduction to N_2 as compared to C_3H_8 pre-treatment: C_3H_6 pre-treatment led to approximately 3 times more deposited carbon as compared to C_3H_8.

The CO and H_2 pre-treatments resulted only in the reduction of surface oxygen and hardly any or no deposited carbon. Therefore, CO and H_2 pre-treatments cannot compete with a hydrocarbon pre-treatment. Deposited carbon, acting as a reductant buffer, extended the period in which NO can be reduced into N_2. C_3H_6 will be preferred over C_3H_8 due to its higher reactivity and increased tendency to form carbon deposits.

5. Conclusion

1) The reduction degree of ceria obtained by C_3H_6 and C_3H_8 reduction, corresponded to up to 2.7 hypothetical reduced ceria layers. As compared to H_2 and CO, the obtainable reduction degrees for these hydrocarbons were around 3 times higher at 580 °C (Table 2). Pre-treatment by C_3H_6 due to its higher reactivity will be preferred over that of C_3H_8.
2) Hydrocarbon pre-treatment led to carbon deposits on the reduced ceria surface. Not the deposited carbon, but the depletion and availability of surface active oxygen species were the main causes for the deactivation of hydrocarbon cracking/partial oxidation/dehydrogenation. These carbon deposits will, however, act as a reductant reservoir, leading to a higher number of NO converted molecules (selective re-oxidation of reduced ceria) into nitrogen [9].
3) The deeper degree of reduction of Zr–La doped ceria during reduction by hydrocarbons will be due to the oxidation of deposited (hydro)carbon intermediated by additional lattice oxygen on the reduced ceria to CO. For H_2 and CO pre-treatment, the apparent existence of H_2, H_2O, Ce^{3+} and Ce^{4+} (or CO, CO_2, Ce^{3+} and Ce^{4+}) equilibrium will limit the ceria reduction of to only one monolayer.

For practical application of ceria-based catalysts in Di-Air system, it might be beneficial to add promoters (for example noble metals) that allow these catalysts to convert hydrocarbons introduced by high frequent fuel injections at lower temperatures.

Acknowledgement

The authors acknowledge financial support from the China Scholarship Council (CSC).

References

[1] Air quality in Europe – 2015 report. http://www.eea.europa.eu/publications/air-quality-in-europe-2015#tab-data-references.
[2] Real-World exhaust emissions from modern diesel cars. http://www.theicct.org/real-world-exhaust-emissions-modern-diesel-cars.
[3] Commission welcomes Member States' agreement on robust testing of air pollution emissions by cars. http://europa.eu/rapid/press-release-IP-15-5945-en.htm.
[4] Y. Bisaiji, K. Yoshida, M. Inoue, K. Umemoto, T. Fukuma, SAE Int. J. Fuels Lub. 5 (2012) 380.
[5] M. Inoue, Y. Bisaiji, K. Yoshida, N. Takagi, T. Fukuma, Top. Catal. (2013) 1.
[6] H.C. Yao, Y.F.Y. Yao, J. Catal. 86 (1984) 254.
[7] C.E. Hori, H. Permana, K.S. Ng, A. Brenner, K. More, K.M. Rahmoeller, D. Belton, Appl. Catal. B 16 (1998) 105.
[8] L. Katta, P. Sudarsanam, G. Thrimurthulu, B.M. Reddy, Appl. Catal. B 101 (2010) 101.
[9] Y. Wang, J. Posthuma de Boer, F. Kapteijn, M. Makkee, ChemCatChem 8 (2016) 102.
[10] Y. Wang, J.P. de Boer, F. Kapteijn, M. Makkee, Top. Catal. 59 (2016) 854.
[11] J. Gleaves, J. Ebner, T. Kuechler, Catal. Rev. Sci. Eng. 30 (1988) 49.
[12] T. Staudt, Y. Lykhach, N. Tsud, T. Skala, K. Prince, V. Matolín, J. Libuda, J. Catal. 275 (2010) 181.
[13] K. Otsuka, Y. Wang, E. Sunada, I. Yamanaka, J. Catal. 175 (1998) 152.
[14] G. Centi, S. Perathoner, ChemSusChem 3 (2010) 195.
[15] C. Padeste, N. Cant, D. Trimm, Catal. Lett. 18 (1993) 305.
[16] B. Murugan, A.V. Ramaswamy, J. Am. Chem. Soc. 129 (2007) 3062.

[17] M.S. Palmer, M. Neurock, M.M. Olken, J. Am. Chem. Soc. 124 (2002) 8452.
[18] Y.-X. Zhao, X.-N. Wu, J.-B. Ma, S.-G. He, X.-L. Ding, Phys. Chem. Chem. Phys. 13 (2011) 1925.
[19] G. Emig, H. Hofmann, J. Catal. 84 (1983) 15.
[20] L.E. Cadus, O.F. Gorriz, J.B. Rivarola, Ind. Eng. Chem. Res. 29 (1990) 1143.
[21] M. Pereira, J. Orfao, J. Figueiredo, Appl. Catal. A 184 (1999) 153.
[22] C. Nederlof, F. Kapteijn, M. Makkee, Appl. Catal. A 417–418 (2012) 163.
[23] P. Albers, J. Pietsch, S.F. Parker, J. Mol. Catal. A: Chem. 173 (2001) 275.
[24] M. Zboray, A.T. Bell, E. Iglesia, J. Phys. Chem. C 113 (2009) 12380.
[25] C. Li, Q. Xin, X.-x. Guo, Catal. Lett. 12 (1992) 297.